ACS Catalysis

pubs.acs.org/acscatalysis
Research Article

Reprogramming the Cyclization of the Sesquiterpene Synthase BcBOT2 Using 2,3-*Z*-Configured FPP Derivatives and by Means of "Methyl Mapping"

Jan Luca Budde, Muhammed-Yasin Çay, Gerald Dräger, Jörn Droste, Ahmed Hassanin, Mehdi D. Davari, and Andreas Kirschning*

Cite This: *ACS Catal.* 2025, 15, 8125−8139
Read Online

ACCESS | Metrics & More | Article Recommendations | Supporting Information

ABSTRACT: The fungal sesquiterpene synthase BcBOT2 shows unique substrate promiscuity. It transforms farnesyl pyrophosphate (FPP) into presilphiperfolan-8β-ol via a cationic cascade that is initiated by a (1 → 11) cyclization. Here, it is shown that BcBOT2 also accepts (2,3-*Z*)-configured FPP derivatives, which provide terpenoids that result from an initial (1 → 6) cyclization. "Methyl mapping" was conducted by shifting the position of one or more methyl groups, and it was found that the location of methyl groups has a profound effect on the efficacy of cyclizations. In particular, the shift of the methyl group at C3 to the C2 position has the most profound effect on cyclohexane formation. Molecular modeling studies show that (1 → 6) cyclization took place due to adopting a different catalytically competent docking pose of FPP derivatives compared to natural FPP within the active site of the BcBOT2, which is mainly due to the (2,3-*Z*)-configuration. This docking pose leads to a C1−C6 distance shorter (3.3−3.5 Å) than the typical association with a near-attack conformation required for cyclization. Finally, these biotransformation results were benchmarked by a comprehensive study of the "hydrolysis" of eight different FPP derivatives. Under enzyme-free conditions, cyclohexene and cycloheptene terpenoids are formed. The ring size is mainly determined by the position of the methyl group at C6 or C7. The study reveals that in addition to protein engineering, unnatural substrates can also be used to specifically manipulate the mode of cyclization of terpene synthases.

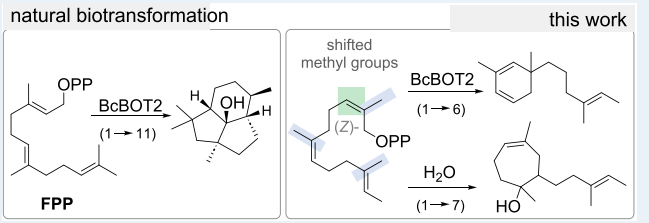

KEYWORDS: *biotransformations, computational modeling, sesquiterpene, sesquiterpene synthases, terpenoids*

INTRODUCTION

In recent years, carbocations and, in particular, the control of cationic cascades have attracted renewed interest. In this respect, nature is proving to be an excellent "chemist" with almost perfect command over cationic cascades, *e.g.*, in the creation of the steroid scaffold by the enzyme lanosterol synthase (LAS).[1−3] Such cascades have been probed by synthetic chemists, and the early work by Johnson,[4,5] Corey,[6,7] and later by Ishihara[8] can be taken as important examples. Their work mainly mimicked oxidosqualene or hopane synthases, which are so-called type II synthases.

Recently, the focus shifted toward chemically mimicking type I terpene synthases.[9−13] Probably most advanced in this respect is Tiefenbacher's approach, which relies on supramolecular capsules bearing a chemically active hollow capsule that is able to promote cationic cascade reactions similar to mono- and sesquiterpene synthases; however, at this point, not with complete enantiocontrol.[14]

In parallel to this development, terpene synthases (TSs), particularly type I members, have attracted interest in chemobiosynthetic transformations using unnatural substrates to access new terpene backbones,[15] which in part has been accompanied by specific amino acid exchanges in the active site of TSs.[16−18]

TSs utilize linear unsaturated methyl-branched precursors activated as diphosphate esters.[19] The protein accommodates the substrate by actively binding the diphosphate moiety through two or three Mg^{2+} cofactor ions. In addition, it supports the folding of the hydrocarbon part of the precursor. A telling example is the sesquiterpene synthase (STS) presilphiperfolan-8β-ol synthase (BcBOT2), a fungal sesquiterpene synthase from *Botrytis cinerea*. It is able to generate the tricyclic sesquiterpene presilphiperfolan-8β-ol (**2**) from farnesyl pyrophosphate ((*E*,*E*)-FPP, **1**) (Scheme 1A). The initial step after diphosphate activation is a (1 → 11) ring closure (Scheme 1A).[20]

Received: February 17, 2025
Revised: April 17, 2025
Accepted: April 23, 2025
Published: May 1, 2025

https://doi.org/10.1021/acscatal.5c01224
ACS Catal. 2025, 15, 8125−8139

Scheme 1. (A) BcBOT2-Promoted Transformation of FPP 1 to Sesquiterpene 2. (B) BcBOT2-Promoted Transformation of "FPP-Ether" 3 to Sesquiterpenoid 4. (C) Isomerization of (*E*,*E*)-FPP 1 to Rotamers 5b or 6, Respectively, via Allyl Cation 5a

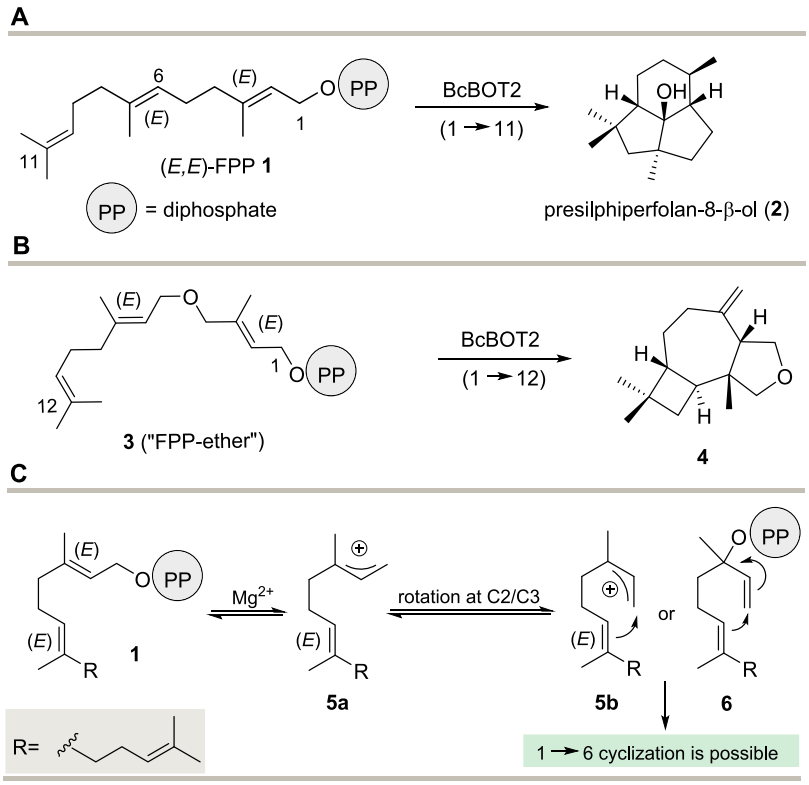

Our studies on the promiscuity of TSs, particularly sesquiterpene synthases, showed that BcBOT2 is able to accept a wide range of non-natural FPP derivatives.[21−28] For example, the transformation of the FPP-ether **3**, prepared by chemical synthesis, which is transformed into the tricyclic terpene furan **4** (Scheme 1B).[21−28] In this case, the transformation is not initiated by a (1 → 11) but rather a (1 → 12) cyclization. Only in a few other cases[29] cyclodecanes are initially formed, but smaller ring sizes have never been reported so far.

A detailed analysis of the product spectrum formed by BcBOT2 with **1** revealed up to 15 other byproducts present in small or minute amounts (0.1−1.6%). Byproducts unequivocally identified were *β*-caryophyllene and its (aut)oxidation product, as well as *β*-elemene, the Cope rearrangement product of thermolabile germacrene A, presilphiperfol-7-ene, (*E*)-*β*-farnesene, and (*E*)-nerolidol.[29] None of these products originate from an initial (1 → 6) cyclization. For smaller rings to initially occur, the allylic pyrophosphate **1** must first isomerize via **5a** and rotamer **5b** or allyl pyrophosphate **6** prior to ring closure, as known from monoterpene synthases (Scheme 1C).

The present work describes how BcBOT2 becomes an efficient STS for (1 → 6)-cyclizations by using differently designed FPP derivatives as a new type of substrates. The study also includes a so-called "methyl mapping", in which the positions of the methyl groups at the three olefinic double bonds are shifted to investigate the influence of the substitution pattern on the cyclization process.

MATERIALS AND METHODS

General Information. ^{1}H NMR spectra were recorded at 400 MHz with a Bruker Avance-400 and Bruker Ascend-400, as well as at 500 MHz with a Bruker DRX-500 spectrometer or at 600 MHz with a Bruker Ascend-600 or Bruker Avance III-600 at 298 or 280 K for low-temperature NMR measurements. ^{13}C NMR spectra were recorded at 100 MHz with Bruker Avance-400 and Bruker Ascend-400 or at 125 MHz with a Bruker DRX-500 or at 151 MHz with a Bruker Ascend-600/Avance III-600 instrument. ^{31}P NMR spectra were recorded at 162 MHz with a Bruker Avance-400 and Bruker Ascend-400. Data analysis was performed by using the Mestrelab Mestrenova software.

Gas chromatography−mass spectrometry (GC-MS) analyses were carried out with an Agilent 7890B GC with 5977B GC-MSD and a Gerstel MPS Robotic XL with KAS 4C injector. Samples were analyzed using an Optima 5HT column, 30 m × 250 *μ*m i.d. × film thickness 0.25 *μ*m. For additional information on the temperature gradient and the detector used, see the Supporting Information. Further GC-MS analyses were carried out with an Agilent GC 7890B chromatograph with a Gerstel CIS4 Cold Injector.

High-resolution GC-MS analyses were carried out on a Waters GCT Premier mass spectrometer coupled with an Agilent 6890n GC with a CTC CombiPAL sampler. HRCI/MS was performed with an HP 6890 Series GC system by Hewlett-Packard.

HR-ESI-MS (Tof) analyses were performed with Alliance 2695 high-performance liquid chromatography (HPLC) (Waters) coupled to an LCT premier (Waters) with a lock spray dual ion ESI source.

https://doi.org/10.1021/acscatal.5c01224
ACS Catal. 2025, 15, 8125−8139

For detailed experimental procedures on the synthesis of FPP derivatives **13**−**19**, refer to the Supporting Information.

Genes, Strains, and Growth Conditions. The gene used in this work was synthesized by GENEWIZ LLC as a construct with pUC57 and is optimized for expression in *Escherichia coli*. The protein sequence can be obtained via the gene bank accession number BcBOT2 (Q6WP50). *E. coli* cultures were grown at 37 °C and 180 rpm in Luria−Bertani medium (LB medium) supplemented with 50 μg mL^{-1} kanamycin. For heterologous expression, 2TY medium supplemented with 50 μg mL^{-1} kanamycin was inoculated by 2% preculture of *E. coli* BL21 (DE3) and grown at 37 °C and 180 rpm to an optical density (OD_{600}) of approximately 0.6. Then, the expression controlled by the T7lac-promotor was induced by adding 0.5 mM isopropyl-β-thiogalactopyranoside (IPTG), and the temperature was decreased to 16 °C for overnight cultivation. Subsequently, the media was removed by centrifugation, and the cells were stored at −20 °C or used immediately. After cell lysis, standard protein purification of histidine-tagged BcBOT2 was performed using Ni-NTA agarose.

Enzyme Assay. The desired FPP derivative (150 μM), along with 0.1 g/L BcBOT2, 50 mM HEPES, 5 mM DTT, and 5 mM $MgCl_2$ (aq), was added to a small glass vial, bringing the total volume to 500 μL. The mixture was incubated at 37 °C and 200 rpm for 30 min. Subsequently, 100 μL of hexane or pentane was added. The vial was vortexed for 30 s. Afterward, the layers were separated again by careful centrifugation (max. 2000 rpm for 4 min). The upper organic layer was then transferred to a GC-inlet vial using Eppendorf pipettes. The sample was then immediately submitted to GC-MS.

General Procedures. *Pyrophosphorylation.* To a solution of tris(tetra-*n*-butylammonium)hydrogenpyrophosphate (2 equiv) and 3 Å molecular sieves in MeCN (50 mM) was added a solution of the respective farnesyl halide derivative (1 equiv) dissolved in MeCN (100 mM) at 0 °C. The mixture was allowed to reach rt overnight. Subsequently, the stir bar as well as the molecular sieves were removed and the solution was concentrated under reduced pressure. A DOWEX column (in the proton state) was flushed with 6% ammonia solution until the eluent showed a pH of 11. Afterward, the resin was washed with distilled water until the eluent was neutral again, followed by washing with an ion exchange buffer (980 mL of water combined with 20 mL of isopropanol and 2 g of NH_4HCO_3). The crude pyrophosphate is then loaded onto the exchange column. The round-bottom flask was rinsed with an ion exchange buffer, which was also loaded onto the column. The ion exchange buffer was used to elute the pyrophosphate. All fractions that stained white/yellow with a common permanganate stain were combined. After the ion exchange was done, the resin in the column was restored by washing with 3 M HCl until the eluent turned acidic. Subsequently, it was flushed with water until the eluent turned neutral again and stored under water until the next usage. The combined fractions containing the desired pyrophosphate were concentrated under reduced pressure. The residue was then dissolved in 1 mL of an aqueous NH_4HCO_3 (0.05 M) solution. The clear solution was transferred to a falcon tube, and 10 mL of a mixture of MeCN and isopropanol (1:1) was added. The suspension was vortexed, followed by centrifugation. The supernatant was collected and the residue was redissolved in 1 mL of an aqueous NH_4HCO_3 (0.05 M) solution. The precipitation was repeated once more with 10 mL of a mixture of MeCN and isopropanol (1:1). The combined supernatants were concentrated under reduced pressure. The pyrophosphate was then transferred into the desired container for storage using water as a solvent. Upon freeze-drying, the desired ammonium pyrophosphate is obtained as a white or yellow gum.

Preparative Biotransformation. To isolate and elucidate the novel biotransformation products, the enzyme assay was scaled up. Therefore, HEPES (50 mM), DTT (5 mM), NaCl (50 mM), and $MgCl_2$ (10 mM) were added to a 100 mL Erlenmeyer flask. The pH was adjusted to 7.5, using NaOH (1 M). Subsequently, the desired pyrophosphate (1 mM) and BcBOT2 (0.1 g/L) were added to the solution. At last, Tween 20 (0.02% [v/v]) and pyrophosphatase (1U) were added to prevent enzyme precipitation and inhibition by abiotic pyrophosphate residues. The amount was calculated for a total volume of 25 mL. The entire procedure was performed a second time, and both Erlenmeyer flasks were closed and placed in an incubator (37 °C, 100 rpm, 24 h). Afterward, the aqueous solutions were combined and extracted with *n*-pentane several times. After sufficient drying of the pentane layer, the solution was concentrated using a constant stream of argon. Purification of the compounds proceeded via column chromatography (SiO_2, *n*-pentane/Et_2O).

Preparing NMR Samples of Volatile Products. The product-containing fractions from column chromatography were combined and concentrated to a volume of 50 μL by using a gentle stream of argon gas. To prevent product evaporation, 1 mL of deuterated benzene was added to the vial. The mixture was then reconcentrated to 50 μL under a light stream of argon gas. The cooling effect of solvent evaporation minimizes the product loss. Co-evaporation of deuterated benzene with pentane/diethyl ether facilitated the removal of nondeuterated solvents. Finally, 1 mL of deuterated benzene was added again, and the mixture was concentrated one last time to approximately 650 μL before being transferred to an NMR tube.

Hydrolysis of (2,3-Z)-FPP Derivatives. The desired ammonium pyrophosphate (100 mg) and distilled water (10 mL) were added to a microwave tube. After sealing, the mixture was stirred at room temperature for 14 days or heated to 75 °C for 5 days. Following the reaction period, oil droplets formed on the surface of the aqueous phase in all decomposition experiments. The tube was then opened, and the aqueous phase was extracted with *n*-pentane (3 mL × 50 mL). The combined organic layers were dried, and purification of the product mixture proceeded via column chromatography (SiO_2, *n*-pentane/Et_2O).

Molecular Modeling. All mechanistic-based molecular docking studies were performed using MOE 2024.06.[60] The three-dimensional (3D) structures were constructed using the "Builder" application in MOE and prepared according to the default protocol of ligand preparation in MOE. The X-ray crystal structure of BcBOT2 (PDB ID: 8H6U)[61] has been used for the docking experiment. The initial position of (*Z*,*E*)-FPP **7** was manually modeled and refined by docking. Prior to substrate docking, the active pocket was selected in the receptor molecule where the pyrophosphate of the substrates binds the tri-Mg^{2+} ions. The substrates were docked using the "Dock" tool in MOE. For each of the ligands, 1000 poses were taken into consideration according to London ΔG Score criteria, of which the top 100 poses were selected for visualization based on GBVI/WSA ΔG Score criteria. For all ligands, the "Triangle Matcher" was chosen for placement, and the "Induced Fit" method was used for the refinement of

https://doi.org/10.1021/acscatal.5c01224
ACS Catal. 2025, 15, 8125−8139

Scheme 2. (A) Transformation of (Z,E)-FPP 7 to Sesquiterpenes 2, 8, and 9 Promoted by BcBOT2. (B) STS Cop6 is an Example of a STS that Accepts Both FPP Derivatives 1 and 7

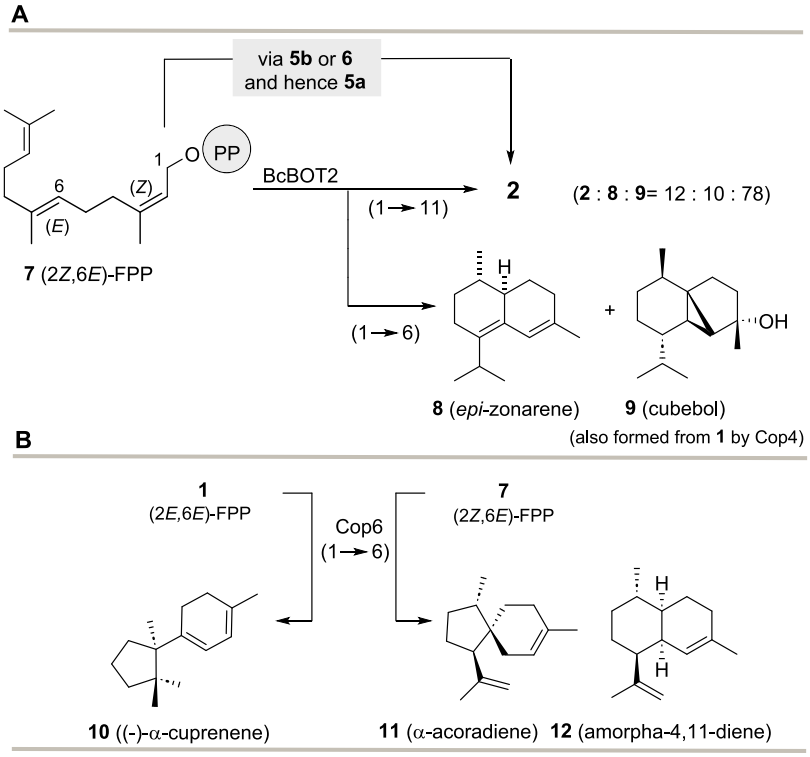

ligand poses, allowing the interaction of flexible side chains at the active site with the substrates.

RESULTS AND DISCUSSION

Preliminary Experiments. In initial investigations using (2Z,6E)-FPP derivative **7** as a substrate, we found that in the presence of BcBOT2, presilphiperfolan-8β-ol (**2**) is also formed; however, only in very small amounts compared to the natural case with FPP **1** (Scheme 2A). Other products identified were *epi*-zonarene **8**[30] and cubebol (**9**).[31−33] The formation of cubebol (**9**) was proven using the retention time collected from GC-MS analysis and direct comparison with authentic cubebol formed from the biotransformation of FPP **1** in the presence of STS cubebol synthase Cop4. Finally, *epi*-zonarene (**8**) was isolated and structurally characterized.

This implies that BcBOT2 is indeed able to catalyze the reversible process described in Scheme 1C (**1** ⇄ **7** likely via **5a**,**b**), though the given stereochemistry at C2 and C3 overwhelmingly determines the mode of the first cyclization step. The literature provides precedence for the substrate promiscuity of STSs with respect to the configuration of the olefinic double bond at C2 and C3. Schmidt-Dannert and co-workers reported that the STSs Cop4 and Cop6, harvested from the fungus *Coprinus cinereus*, are able to accept and convert both FPP stereoisomers (Scheme 2B).[31−33]

Cyclization of (2Z,6E)-FPP **7** by Cop6 yields α-acoradiene **11** and amorpha-4,11-diene **12** that structurally differ from (−)-α-cuprenene (**10**) formed from natural (E,E)-FPP **1**.[31−33] In both cases, the biotransformations are initiated by a (1 → 6) cyclization. Other examples were reported by Degenhardt et al. with the STSs TPS4, TPS6, and TPS11 from maize.[34−36]

From this initial experiment (Scheme 2A), we concluded that FPP derivatives with a (2Z)-configured double bond might serve as potential substrates for BcBOT2. Accordingly, it is conceivable that the intermediates **5a**,**b** should be available for cyclizations when pyrophosphates derived from **7** are employed, paving the way for (1 → 6) or (1 → 7) cyclizations promoted by BcBOT2.

Chemical Synthesis of Substrates. To test this hypothesis, we pursued "methyl mapping" by preparing a series of FPP derivatives **13**−**19** with a (2,3-Z)-configured olefinic double bond (Scheme 3, top). We use the term "methyl mapping," for structural variations that denote the positions of methyl groups along the three olefinic double bonds. Up to three methyl groups were shifted toward the diphosphate terminus. In addition, one derivative **19** carries an additional oxygen functionalization as we recently reported that FPP derivatives with a methoxy group are accepted by STSs.[12d] It is worth noting that we had experienced in other studies before that the delicate methyl shift from C3 to C2 does not inhibit the binding and processing of FPP derivatives by BcBOT2.[37]

The shift of selected methyl groups, especially the central one, implies that ring closure could either proceed via a secondary **B** and **C** or a tertiary carbocation **A** or **D** in case the formation of only one ring size is preferred by BcBOT2 (Scheme 3, bottom). If the stability of the intermediate carbocation governs ring closure, then either cyclohexanes **A** and **B** or cycloheptanes **C** and **D** will be formed first. Thus, the present study not only focuses on the promiscuity of BcBOT2 toward (2,3-Z)-FPP derivatives but also sheds light on factors such as substitution patterns that control the ring closure.

It was found that for the individual (2,3-Z)-FPP derivatives **13**−**19**, depending on the location of the individual methyl groups, individually designed synthetic routes must be developed. This becomes apparent in the choice of the starting

https://doi.org/10.1021/acscatal.5c01224
ACS Catal. 2025, 15, 8125−8139

Scheme 3. Top: FPP Derivatives 13−19 Studied in this Work (the blue labeling of the methyl groups marks their non-natural positioning with regard to the methyl mapping carried out in this work). Bottom: Considerations on Mode of Cyclizations to Intermediate Cations A−D

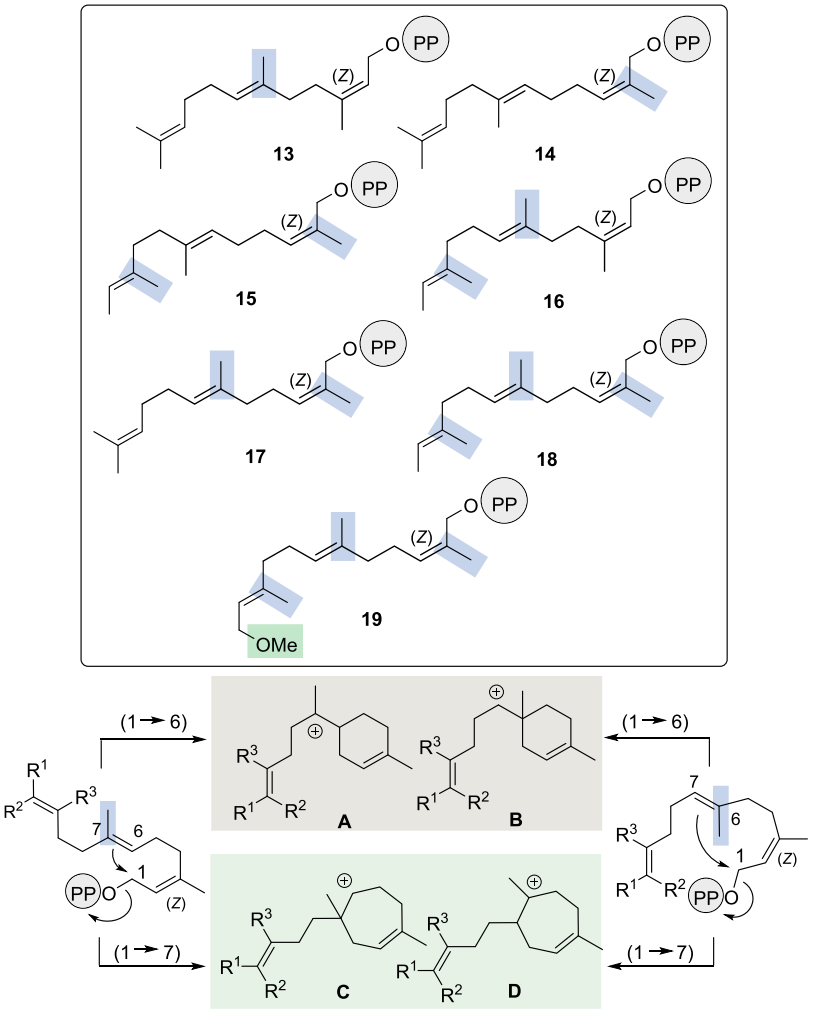

building blocks nerol **20**, geraniol **30**, methacrolein **38**, and farnesol **42**, so that the routes described below are subdivided according to the choice of these building blocks (Schemes 4B and 5A−C). In each case, the aim was to first gain access to the corresponding farnesol derivatives, which were then converted to pyrophosphates by a two-step protocol, according to the report by Poulter et al.[38] (Scheme 4A).

The syntheses of the unnatural (2,3-*Z*)-FPP derivatives **7**, **13**, and **16** with a methyl group located at position C3 commenced with nerol **20** as the starting material (Scheme 4B), which had to be elongated by an additional ispoprene unit, represented by building blocks **27** and **28**, respectively. After *O*-silylation, Riley oxidation, and bromination, the resulting allyl bromide **22** was coupled with sulfone **27** to yield farnesol derivative **23** after desilylation. Phosphorylation, according to Scheme 4A, provided the FPP derivative **7**.

For accessing FPP derivatives **13** and **16**, the terminal dimethyl group present in nerol **20** was removed first. This was achieved by an established oxidative protocol[39] that furnished ketone **24**, which was converted to bromide **25** in a three-step sequence, with Horner−Wadsworth−Emmons olefination serving as the key step. Depending on whether sulfone **27** or bromide **28** is used to introduce the additional isoprenoid moiety, either pyrophosphate **13** or **16** can be made available. Olefination of ketone **24** with phosphonate **29** gave a diastereomeric mixture (4:1) of α,β-unsaturated esters, and the isolated (*E*)-configured ester was subsequently reduced and converted to allyl bromide **25**. From there, coupling with sulfone **27**,[40] reductive removal of the sulfone group,[40] and *O*-desilylation gave the corresponding farnesol derivative. The introduction of the diphosphate moiety finally afforded FPP derivative **13**.

The synthesis of FPP derivative **16** also relied on precursor allyl bromide **25**, which was converted to the respective sulfone through nucleophilic substitution. Bromide **28** served as a coupling partner to yield sulfone **26**. This was converted to FPP derivative **16** according to the sequence described for FPP derivative **13**.

Unnatural (2,3-*Z*)-FPP derivatives **14** and **17**, featuring a methyl group at the C2 instead of C3, were prepared by starting from geraniol **30** (Scheme 5A). Methyl substitution at C2 along with the (2,3-*Z*) configuration was usually installed by means of the (*Z*)-selective Still-Gennari olefination[41] from the corresponding aldehydes using phosphonate **36**. The synthesis of FPP derivative **14** starts with the bromination of **30**, which served as an alkylating agent for acetic acid furnishing ester **31**. Reduction to the corresponding aldehyde paved the way for the *Z*-selective olefination, which provided

https://doi.org/10.1021/acscatal.5c01224
ACS Catal. 2025, 15, 8125−8139

Scheme 4. (A) General Procedure for the Phosphorylation of FPP Alcohol Derivatives. (B) The Synthesis of (2,3-*Z*)-FPP Derivatives 7, 13, and 16 (refer to Supporting Information (SI) for further details)

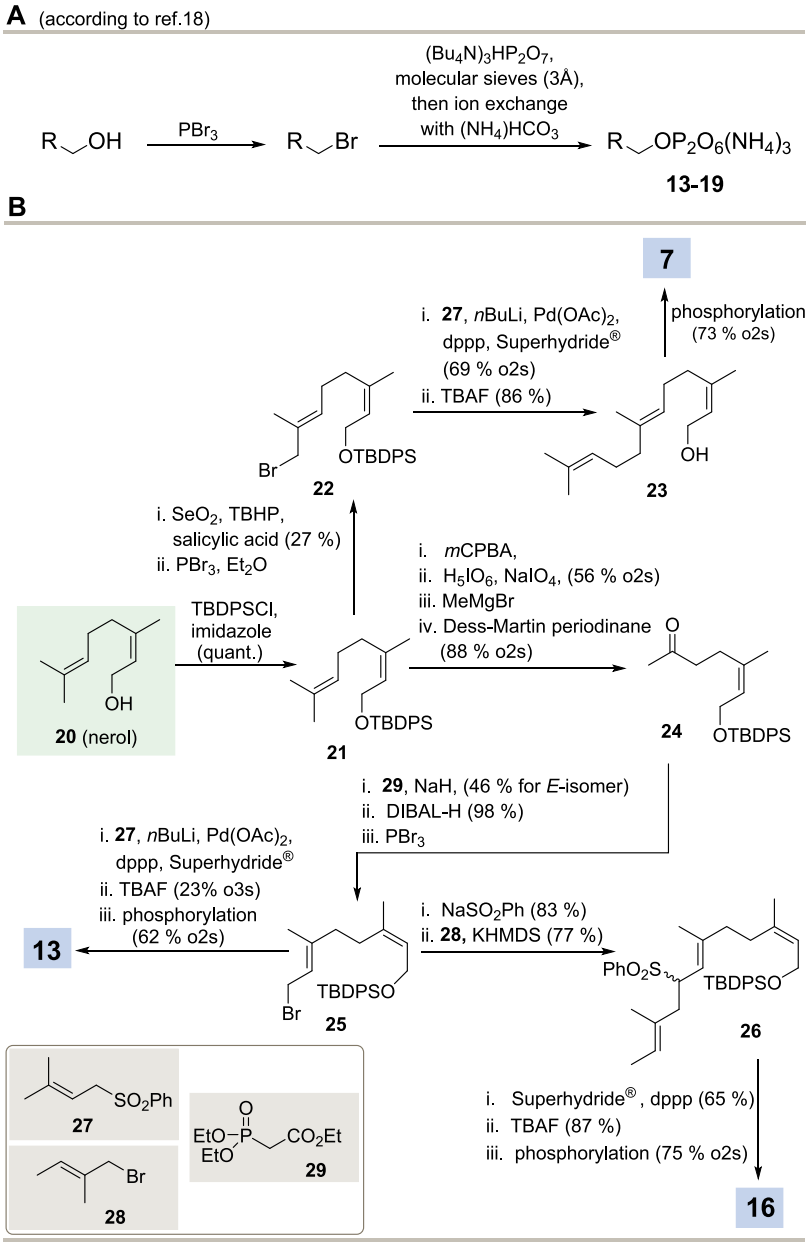

α,β-unsaturated ester **32**. From there, the farnesol derivative serves to introduce the pyrophosphate group under the conditions depicted in Scheme 4A, yielding FPP derivative **14**.

Oxidatively replacing the dimethyl group of geraniol **30** by an aldehyde group using an established protocol[39] provides the starting point for the (*Z*)-selective Still-Gennari olefination, that leads to the allyl alcohol **35** after a three-step protocol of functional group manipulations. Next, the hydroxyl group was transformed into the corresponding chloride, which served as a fragment for coupling with lithiated allyl sulfone **27**. Reductive removal of the sulfone group and removal of the tetrahydropyranyl protection liberated the alcohol group at the other terminus of the carbon backbone. The standard two-step protocol (Scheme 4A) finally furnished FPP derivative **17**.

Due to the methyl groups at positions C7 and C10, alkyl coupling with bromide **28** was not an option for the synthesis of (2,3-*Z*)-FPP derivative **15**, as we experienced the formation of a product mixture upon reductive removal of the sulfone group. As a consequence, the entire backbone had to be constructed de novo, and we chose methacrolein **38** as the starting material (Scheme 5B). It was first methylated, and the alcohol was esterified and rearranged under typical Johnson–Claisen rearrangement conditions using ortho ester **37**.[42]

The resulting ester was methylated, and the intermediate ketone was subjected to a Horner–Wadsworth–Emmons olefination, which furnished ester **39** as a separable mixture of stereoisomers as expected for ketones. Using the (*E*)-isomer, the final steps toward farnesol derivative **41** proceeded via ester **40**, which was reduced, and the corresponding aldehyde was subjected to a Still-Gennari olefination, which established the (2,3-*Z*)-configured alkene. Finally, the established phosphorylation furnished FPP derivative **15**. In the two (2,3-*Z*)-FPP derivatives, **18** and **19** methyl groups are shifted by one position around all alkenes. The most effective way to

https://doi.org/10.1021/acscatal.5c01224
ACS Catal. 2025, 15, 8125−8139

Scheme 5. (A) Synthesis of (2,3-*Z*)-FPP Derivatives 14 and 17. (B) The Synthesis of (2,3-*Z*)-FPP Derivative 15. (C) The Synthesis of (2,3-*Z*)-FPP Derivatives 18 and 19 (refer to the SI for further details)

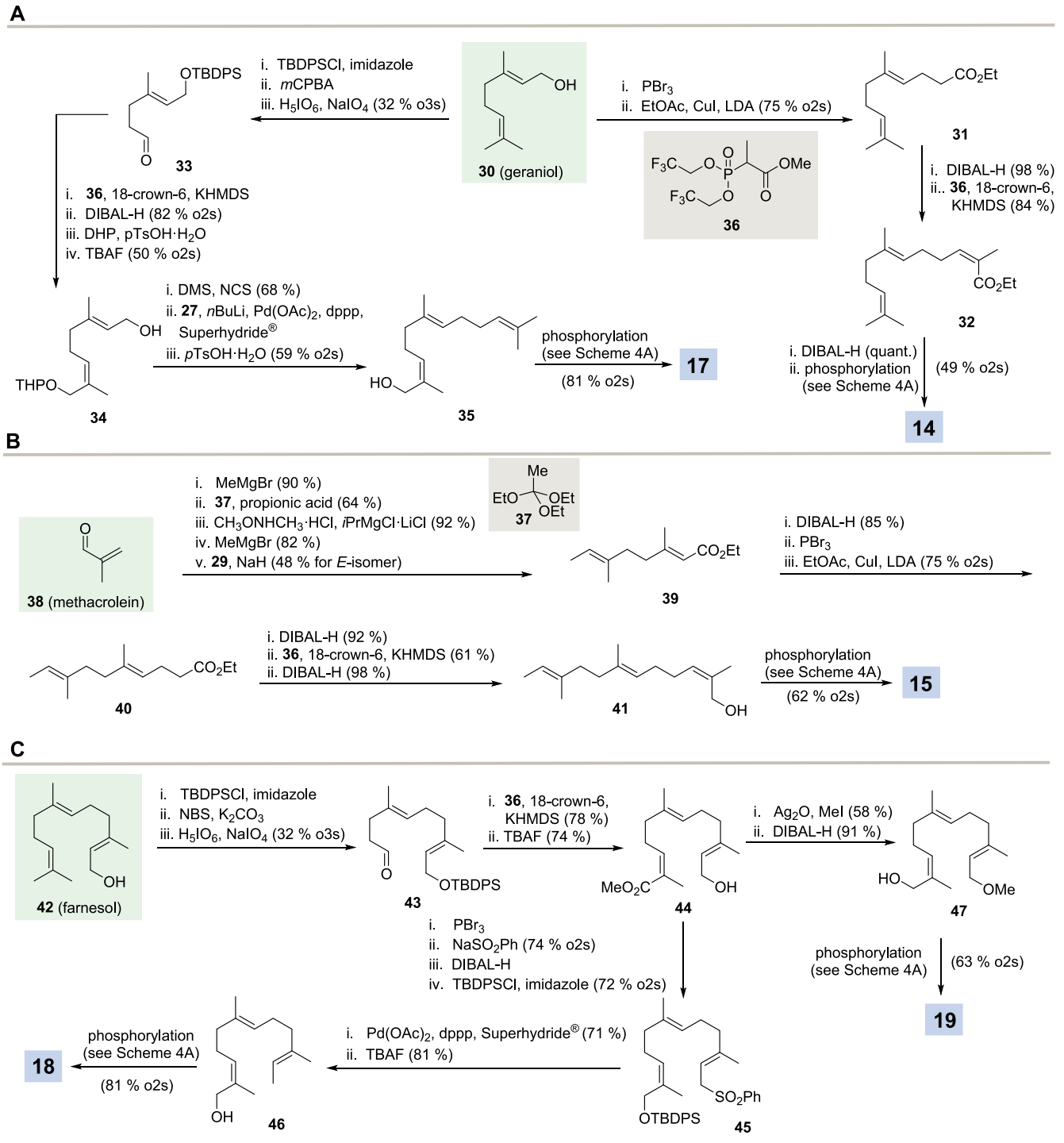

construct this unusual backbone was by installing the pyrophosphate group at the dimethyl terminus of farnesol **42** (Scheme 5C). This was achieved by oxidative removal of this terminus,[39] and the resulting aldehyde **43** was subjected to the Still-Gennari olefination conditions[41] using phosphonate **36**. The resulting ester **44** is the branching point for preparing FPP derivatives **18** and **19**. The former derivative was accessed by OH → Br exchange and sulfonation. The ester terminus was next reduced to the alcohol and silyl protected. This paved the way to reductively remove the sulfone and establish the 1,2-dimethylated alkene moiety in compound **45**. The last steps follow our established protocol of silyl deprotection, bromination, and introduction of the diphosphate group in FPP derivative **18**. Starting from intermediate **44**, the hydroxyl group was alternatively *O*-methylated, followed by ester reduction (yielded intermediate **47**) and introduction of the diphosphate moiety with the formation of FPP derivative **19**.

Biotransformations. For conducting biotransformations, BcBOT2 was cloned and expressed in *E. coli*. *In vitro* enzyme tests, for determining enzyme activity and for optimizing

https://doi.org/10.1021/acscatal.5c01224
ACS Catal. 2025, 15, 8125−8139

Table 1. Products Formed by BcBOT2 from FPP Derivatives 13−19 (Blue Labeling Marks Unnatural Positioning of Methyl Groups; Green Labeling Marks Additional Functionality)

entry	FPP derivative	products[a]
1	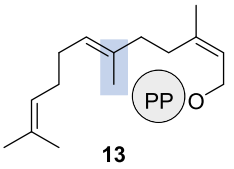 **13**	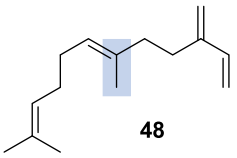 **48**
2	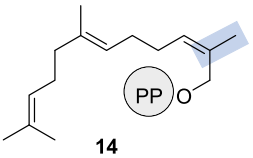 **14**	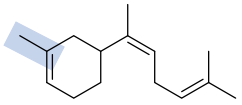 **49** (only product)
3	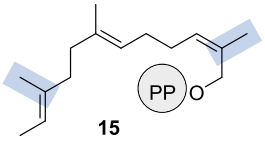 **15**	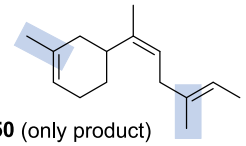 **50** (only product)
4	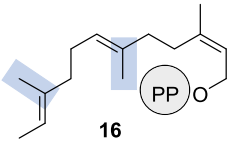 **16**	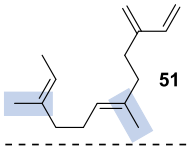 **51**
5[b]	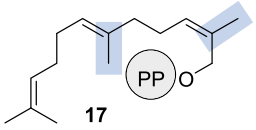 **17**	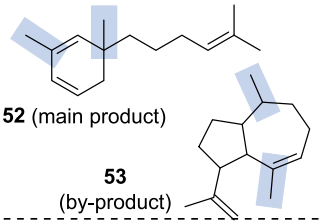 **52** (main product) **53** (by-product)
6	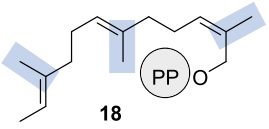 **18**	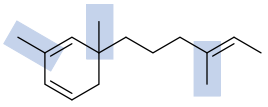 **54** (only product)
7	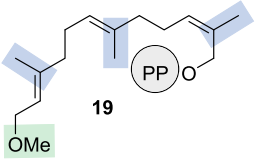 **19** OMe	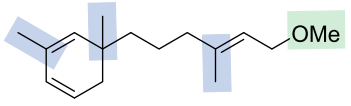 OMe **55** (only product)

[a]For details on the isolation and structure elucidation, see the SI. [b]**52:53** = 3:1.

substrate tolerance, were conducted on small scales (150 μM substrate, 0.1 mg/mL enzyme) using natural precursor FPP **1** (see the SI).

In order to collect sufficient amounts of biotransformation products, the experiments were scaled up to a total volume of 25 mL with some modifications regarding the buffer composition in the presence of FPP derivatives **13−19** (1 mM) and BcBOT2 (0.1 g/L) (see the SI) (Table 1). The biotransformations furnished several new terpenes, some of which share structural similarities to known terpene backbones. The only previously reported product is myrcene derivative **48**, though only mass spectroscopic data were initially published for this farnesene derivative.[43] The structural analysis of the products **48−55** was straightforward and relied on mass spectrometry and NMR spectroscopy (including two-dimensional (2D) techniques that included the nuclear Overhauser effect (NOE) and NOESY experiments to determine double bond geometries). Details are found in the Supporting Information.

https://doi.org/10.1021/acscatal.5c01224
ACS Catal. 2025, 15, 8125−8139

It should first be emphasized that (2,3-*Z*)-FPP derivatives **13**−**19** are principally prone to (1 → 6) cyclizations. In several cases, the cyclohexene terpenoids are formed as the only product (entries 2, 3, 6, and 7, Table 1), in the case of cyclohexadiene derivative **52** (entry 5) as a major product.

FPP derivatives **13** and **16** did not yield any cyclization products (entry 1). The formation of products that would result from initial (1 → 10) or (1 → 11) ring closures was not observed in any of the investigated cases except for the parent derivative (2,3-*Z*)-FPP **7**. This finding confirms the assumption initially made that BcBOT2 is able to accept and cyclize (2,3-*Z*)-FPP derivatives. However, the process differs from that with pyrophosphate **7**, as presilphiperfolan-8β-ol (**2**) is formed, albeit in a poor yield. This tricyclic sesquiterpene could only be formed if one assumes an isomerization, as depicted in Scheme 2. Furthermore, every unnatural (2,3-*Z*)-FPP derivative employed in this study is transformed into the respective alkene, as displayed in Table 1. Even though BcBOT2 transforms FPP **1** into alcohol **2** by trapping the final cation by water, we did not encounter sufficient formation of any alcohol in the present study either by GC-MS analysis or after isolation.

The second aspect of interest is linked to the fact that, regardless of the position of the methyl group on the central alkene moiety (either position 6 or 7), only (1 → 6) cyclization occurs (see also considerations listed in Scheme 3). This indicates that BcBOT2 significantly controls the conformation of the (2,3-*Z*)-FPP derivatives right before the cyclization step. However, it appears that the displacement of individual methyl groups at this and the olefinic double bond at C10,11 has no significant effect on the mode of cyclization (position C in Figure 1). At best, it has a modulating effect on

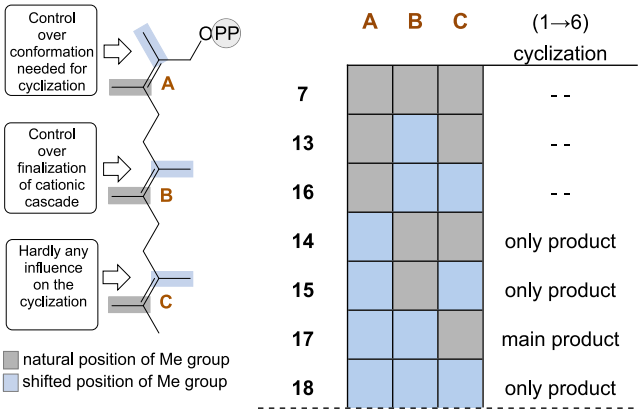

Figure 1. Correlation between the position of the shifted methyl groups in (2,3-*Z*)-FPP derivatives **7** and **13**−**18** and cyclization by BcBOT2.

substrate folding within the enzyme cavity. This is evident if one compares the results collected with FPP derivatives **17** and **18**, with the former yielding several byproducts not observed with substrate **18**. In contrast, the shift of the methyl group from C3 to C2 dramatically fosters (1 → 6) cyclization, which invariably leads to cyclohexenes (see entries 2, 3, and 5−7, Table 1 and Figure 1).

If the methyl group in (2,3-*Z*)-FPP derivatives remains at C3 (entries 1, and 4; Table 1), cyclization occurs inefficiently, if at all, and the process is mainly determined by the cleavage of diphosphate. This is also confirmed by the result with (2,3-*Z*)-farnesyl pyrophosphate (**7**) described above. Again, no (1 → 6)-cyclization products were found. The formation of sesquiterpene **2** in only small amounts indicates that the isomerization process described in Scheme 1C proceeds very slowly compared with elimination or hydrolysis. For the biotransformations of FPP derivatives **13**−**19** with BcBOT2, no cyclization products could be detected that would require prior isomerization. If such products were formed, then only in very small and barely detectable quantities.

As part of the structural analysis, we observed an interesting NMR phenomenon, which will be briefly explained here. The multiplet structure caused by the ^{13}C-^{31}P *J*-coupling observed in the $^{13}C\{^1H\}$ NMR spectra differs for the compounds with the methyl group in position 2 compared to that in position 3. For the 2-methyl derivatives, a doublet is observed for C1 and C2, respectively. In contrast, a triplet-like signal pattern is visible for C1 and C2 in the $^{13}C\{^1H\}$ NMR spectra when the methyl group is positioned at C3, as in derivatives **7**, **15**, and **18**. This is a clear indication of long-range coupling with the second phosphor atom. Since the *J*-coupling value can be related to the bonding angle defined in the Karpus-like equation[44] and, hence, to the difference in the bonding geometry induced by the position of the methyl group. However, a detailed investigation of this effect is beyond the scope of this article and will be described in more detail in due course.

Computational Modeling. To shed light on these observations, we performed mechanism-based substrate docking for (2,3-*Z*)-FPP derivatives **13**−**19**, helping to rationalize the switch of initial ring closure from (1 → 11) to (1 → 6) cyclization. For that, we analyzed the possible binding modes of the substrates in the active site of BcBOT2. It has been reported that the near-attack conformation (NAC) in the catalytically competent pose required for ring closure is defined by the C−C distance of the relevant carbon atoms in the substrate. Previous high-level quantum chemical calculations and structural studies showed that this distance should be shorter than 4.0 Å.[45]

First, the analysis of the binding mode revealed that substrates **13**−**19** have comparable binding free energies (−20 ± 2 kcal/mol). The dominant binding mode of substrates **14** and **15** with a 2,7-methyl substitution reveals C1−C6 distances of 3.35 and 3.46 Å, respectively. This does favor (1 → 6) cyclization. In contrast, no favorable binding mode could be found for the (1 → 11) cyclization pathway (Figure 2). Similar results are also collected for FPP derivatives **17**−**19** with methyl branching at positions 2 and 6. Here, an average C1−C6 distance of 3.33 Å was calculated, which confirms our experimental findings with respect to the mode of cyclization. As such, the favorable impact for (1 → 6) cyclizations is supported when moving the methyl group from position 3 to position 2 (Figure 3).

However, for FPP derivative **17**, there is also a second favorable binding pose favorable for catalysis where the C1−C7 distance is 3.30 Å, which favors the initial (1 → 7) ring closure. Later, a (1,3) hydride shift followed by (1 → 10) cyclization likely would yield the bicyclic skeleton of **53** (Scheme 6B). Our calculations also suggest that the final elimination can be performed by the nearby pyrophosphate moiety (Figure S7; SI).

Finally, for the two FPP derivatives **13** and **16** with methyl groups at positions 3 and 6, our calculations did not reveal a binding mode that would allow cyclization between C1 at the

https://doi.org/10.1021/acscatal.5c01224
ACS Catal. 2025, 15, 8125−8139

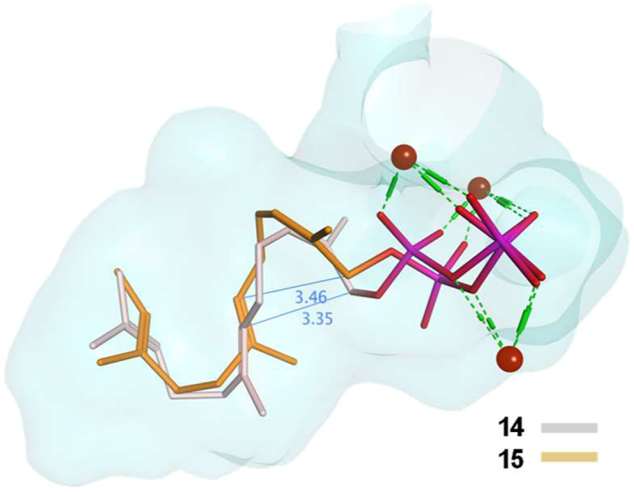

Figure 2. Close-up view of the binding modes of FPP derivatives **14** and **15** within the active site of STS BcBOT2. The 3D representation shows the catalytically competent pose of both substrates with a focus on the ionic interactions between the pyrophosphate moiety and the 3 Mg^{2+} cations. It reveals that the near-attack conformation (NAC) for the C1−C6 distance of about 3.35 and 3.46 Å, respectively, are fulfilled. Detailed docking poses are found in the Supporting Information (Figures S4 and S5, SI).

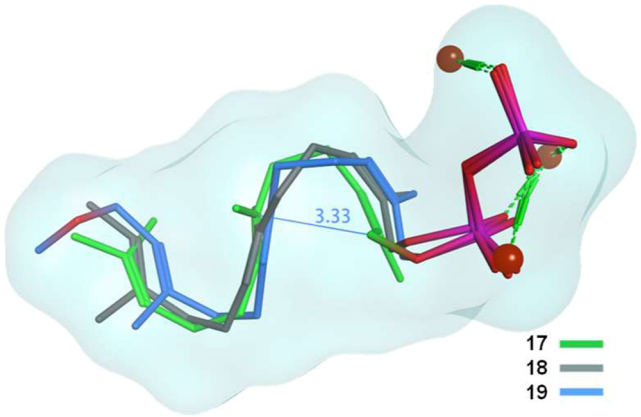

Figure 3. Close-up view of the binding modes of derivatives **17**−**19** within the active site of the STS BcBOT2. The 3D representation shows the catalytically competent pose of the three substrates with a focus on the ionic interactions between the pyrophosphate moiety and the 3 Mg^{2+} cations. It reveals that the near-attack conformation (NAC) for the C1−C6 distance of about 3.35 and 3.46 Å, respectively, are fulfilled. Detailed docking poses are found in the Supporting Information (Figures S6 and S9, SI).

two alkenes at C6,C7 and C10,C11, respectively, for distance reasons. This is additional support for the findings. Details on the analysis of docking poses are found in the Supporting Information (Figure S3, SI).

With reference to previous work in which the (2,3-*E*)-configured FPP with the methyl group positioned at C2 instead of C3 (*i.e.*, the 2,3-*E* isomer of **17**) was employed in biotransformation with BcBOT2, we gain support for our computational calculations that suggest an initial 1 → 7 cyclization (Figures S6 and S7, SI). This *E*-derivative provided the corresponding germacrene derivative formed by a 1 → 10 cyclization. With FPP derivative **17**, we could not detect the formation of this germacrene derivative. This implies that the tendency of BcBOT2 to promote a 2,3-*E*/*Z*-isomerization, as described in Scheme 2A, has no significance in the transformation from **17** to **53**.

Mechanistic Considerations. All products are created by a final deprotonation step and consequently the formation of an alkene moiety, despite the fact that presilphiperfolan-8β-ol (**2**) is the result of water addition. A closer look reveals a diverse pattern for the final elimination. Mechanistically, FPP derivatives with a natural substitution pattern around the central olefinic double bond B (C6,C7) lead to tertiary carbocation **56** and deprotonation exclusively occurs in the neighboring position in the side chain (Scheme 6A, top). As a result, sesquiterpenoids **49** and **50** are formed from FPP derivatives **14** and **15**, respectively. The situation changes when the methyl group at C7 is shifted to C6 (Scheme 5A; bottom). Cyclization again leads to a six-membered ring (governed by the methyl group at C2), but this time, the less stabilized secondary carbocation **57** is formed instead.

It appears that the position of the central methyl group takes control over the deprotonation, thereby determining the outcome of the final double bond pattern. Direct elimination toward the side chain does not take place here. Instead, a 1,3-hydride shift (or alternatively two 1,2-hydride shifts) occurs, and the newly formed allylic carbocation undergoes deprotonation and cyclohexadiene formation. This transformation was proven for the FPP derivatives **17**−**19**, all of which have the methyl group at C6 instead of C7. Consequently, terpenoids **52**, **54**, and **55** are formed.

Only in one case did we observe an initiating (1 → 7) cyclization with BcBOT2, starting from FPP derivative **17** (Scheme 6B). It led to the formation of the sesquiterpene **53** that bears a bicyclo[5.0.3]decane backbone. The first step yields the thermodynamically more stable tertiary carbocation **58**, which, after a 1,3-hydride shift, forms cation **59**, and a second cyclization combined with deprotonation provides terpenoid **53** (Scheme 6B). Bicyclo[5.0.3]decane-bearing sesquiterpenes are often listed in the class of guaiane sesquiterpenes,[46] A typical example is pogostol **60** with a substitution pattern at the bicyclic system represented by structure **I**. The simplified structure **II** reveals that **53** has a substitution pattern different from the natural guaiane sesquiterpenes.[47] Finally, the isolation of elimination products **48** and **51** indicates that the deprotonation is controlled by the template. The diphosphate anion in the active center of the synthase probably acts as a base and thus determines the site of deprotonation, as alternative myrcene-type products were not found (Scheme 6C).

These mechanistic observations are supported by the *in silico* modeling studies where mechanistic-based molecular docking was carried out for the carbocationic intermediates **56** and **57** (see above). For intermediate **56**, it is more likely for C8 to undergo deprotonation promoted by Tyr335 being located as close as 2.4 Å than to undergo a hydride shift. However, for **57**, this Tyr335 is positioned further away so that a 1,2-hydride shift is more likely to occur, which is followed by deprotonation at C4 by the diphosphate moiety (Figure S10, SI).

The structure−reactivity trends outlined above currently apply only to sesquiterpene synthase BcBOT2. However, it is very plausible that similar observations will be found for other terpene synthases, provided they can process these unnatural (2,3-*Z*)-FPP derivatives. Nevertheless, the high selectivity toward single-product formation is likely a distinctive feature

https://doi.org/10.1021/acscatal.5c01224
ACS Catal. 2025, 15, 8125−8139

Scheme 6. (A) Mechanistic Consideration on the Formation of Cyclohexenes and Cyclohexadienes. (B) Mechanistic Considerations on the Formation of Cycloheptene 53 and Comparison with Related Skeletons I and II of Natural Terpenoid; (C) Controlled Formation of Myrcene Derivatives 48 and 51

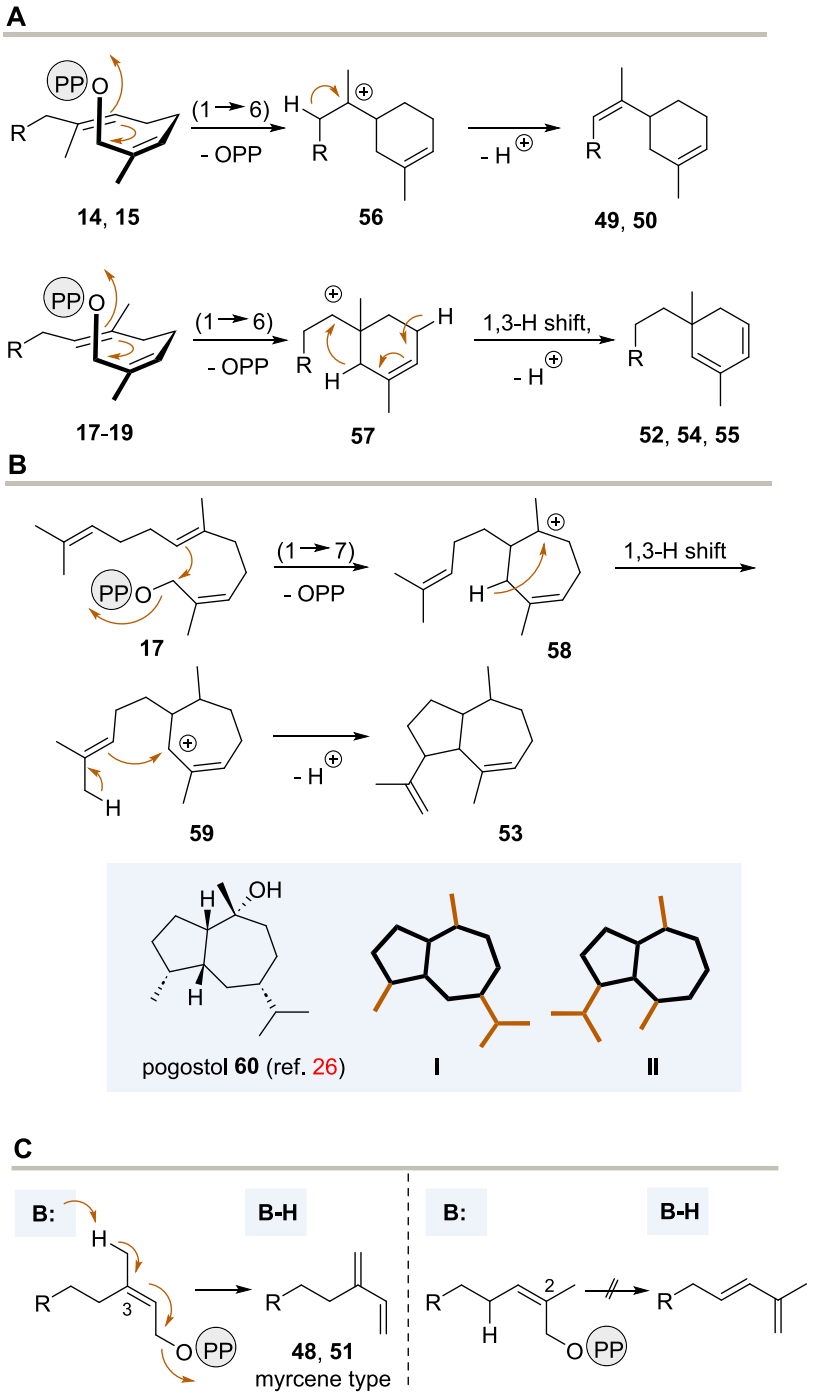

of the specific interaction between BcBOT2 and the unnatural FPP derivatives **13**−**19**.

"Chemical Hydrolysis". In parallel to the biotransformations summarized in Table 1 and Figure 1, we studied the fates of FPPs **1** and **7** as well as the new derivatives **13**−**19** under neutral aqueous conditions in the absence of BcBOT2 (Figure 4). These experiments should unequivocally verify that the formation of new cyclohexyl terpenoids is driven by BcBOT2. Initially, these studies were carried out with FPP **1** and (2,3-*Z*) isomer **7**, as surprisingly little information about the "hydrolysis" of isoprenoid pyrophosphates can be found in the literature.

In 1977, Brody and Gutsche reported on the acid-mediated decomposition of pyrophosphates **1** and **7**.[48] Contrary to these conditions, we employed neutral aqueous conditions (pH 7) to more closely mimic our biotransformations. It needs to be noted that the addition of magnesium chloride did not alter the outcome of these reactions (Figure 2). Besides the expected linear products (nerolidol, farnesol, and myrcene) also, the formation of two (1 → 6) cyclization products, namely, *α*-bisabolol **62** and *β*-bisabolene **63**, were detected. Brody and

https://doi.org/10.1021/acscatal.5c01224
ACS Catal. 2025, 15, 8125−8139

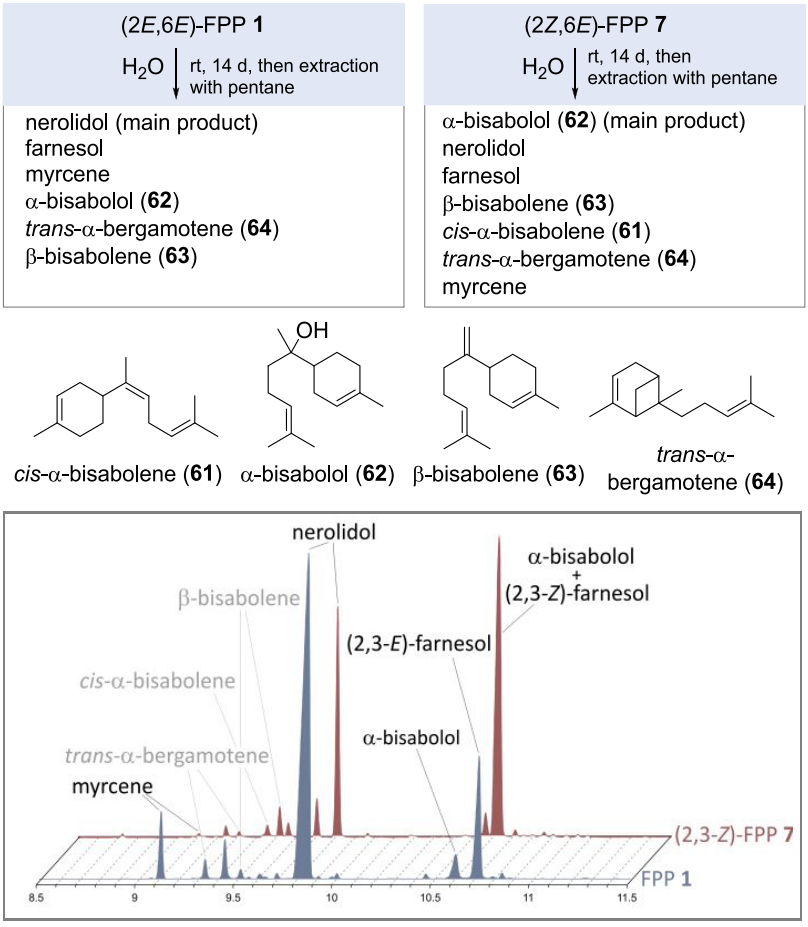

Figure 4. "Hydrolysis" of FPP **1** and the (2,3-*Z*)-isomer **7** (the lists are ordered from top to bottom with decreasing GC signal intensity). Products displayed in gray were identified by MS comparison to the NIST-WebBook database.

Gutsche also reported[48] that nerolidol was the main "hydrolysis" product obtained from **1** as well as bisabolol, a cyclization product that preferentially forms from **7**. The FPP derivatives **1** and **7** yield almost the same set of products under the conditions employed in our work. Hydrolysis experiments with newly synthesized (2,3-*Z*)-FPP derivatives **13**−**19** (Table 2) resulted in a variety of ring sizes and unconventional nerolidol derivatives. All isolated hydrolytic products (**65**−**74**) are novel and have not been previously reported. Furthermore the hydrolysis experiments also revealed several trends. The (2,3-*Z*)-FPP derivatives **13** and **16** with the methyl group positioned at C3 proved to be more labile under the hydrolytic conditions than the derivatives **14**, **15**, and **17**−**19** that have a methyl group positioned at C2. We first noticed the differences in hydrolytic stability during NMR measurements in D_2O. Consequently, NMR analytics had to be carried out at a lower temperature (280 K). Under these conditions, we also detected the formation of substantial amounts of the allyl alcohols **69**, **72**, and **74**.

In contrast to BcBOT2-mediated cyclizations, the location of the methyl group at C6 or C7 expectedly has an overriding influence on the ring size that is formed. It always proceeds via a more stable intermediate carbocation.

Thus, cyclohexenes **65** and **66** are formed from precursors **14** and **15** with the methyl group positioned at C7, while cycloheptenes **67**, **68**, **70**, **71**, and **73** are obtained from the FPP derivatives **13**, **16**−**19** with the methyl group located at C6.

Overall, the experiments reveal, for the first time, on a preparative scale, the product spectrum that is formed during the hydrolysis of FPP derivatives. They provide proof that such substrates yield ring-closed products even without template control exerted by synthases. These findings could provide insight into the development of chemical mimics of terpene synthases.[9−13] Noteworthily, the formation of cyclohexenes under aqueous conditions does not proceed in a stereocontrolled manner, as is evident from the formation of two diastereomers.

In contrast, cycloheptenes are commonly isolated as a single diastereomer. This observation can be ascribed to the conformation of the intermediate tertiary carbocation. In the case of cyclohexene formation, the final carbocation is located in the side chain, while cycloheptene formation proceeds via a carbocation located in the 7-membered ring. It can be assumed that the conformation of the aliphatic side chain provides a facial bias for water addition.

CONCLUSION

The present work illustrates that not only changes in the protein sequence (by mutation) of terpene synthases can serve as a strategy to manipulate the cationic mechanism of TSs,[16−18,48] but that also the design of new substrates can lead to a completely new "chemical behavior" of TSs as exemplified for BcBOT2 here. Besides alkene configuration, "methyl mapping" provides an opportunity to control substrate conformation prior to the initial cyclization step, which is

https://doi.org/10.1021/acscatal.5c01224
ACS Catal. 2025, 15, 8125−8139

Table 2. Cyclizations of (*Z*,*E*)-FPP Derivatives 13−19 under "Hydrolytic" Conditions[a]

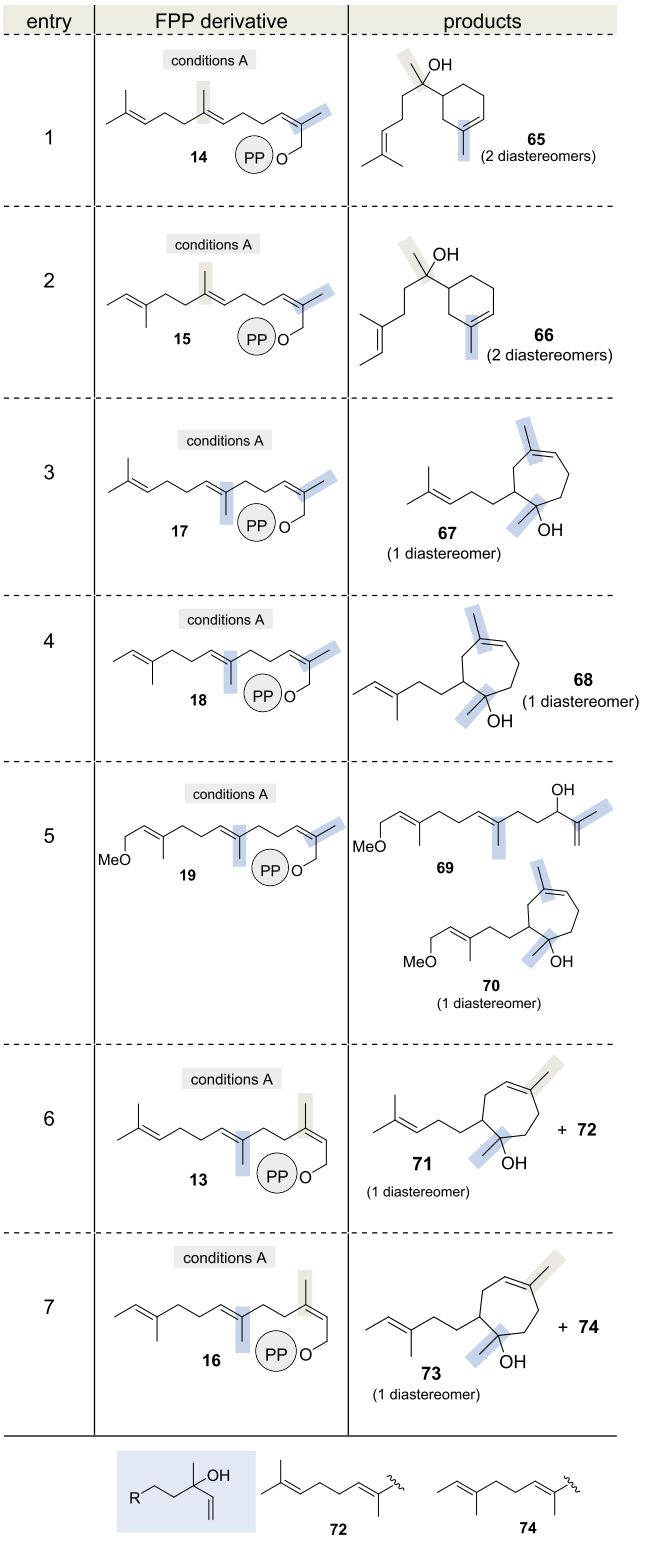

[a]Conditions A: H_2O, rt, 14 d, and then pentane extraction, B: H_2O, 75 °C, 5 d, and then pentane extraction.

supported by our molecular modeling studies. As a result, a shorter C−C distance is generated, paving the way for cyclohexene formation. TSs have occasionally been regarded as hydrophobic molds that merely form a template for the already highly favored cascade reaction in the absence of enzymes and water. The highly reactive carbocation initially formed is the driving force.[49−51] However, TSs do indeed achieve a specificity that far exceeds or is solely determined by intrinsic reactivity, as is demonstrated here.[52−58] In the context of this discussion, our "hydrolysis" experiments are therefore important because they allow us to estimate the influence of the STS BcBOT2 on both the acceleration and the progression of cyclization compared to water alone. Methyl mappings and/or shifts of alkene positions are, in principle, capable of encoding different cyclization outcomes without the need for individually tailored catalysts, as recently discussed in a manuscript dealing with computational predictions of cationic cascades.[59] In contrast, BcBOT2 still seems to largely override this substrate preference by controlling the conformation.

■ ASSOCIATED CONTENT

Supporting Information

The Supporting Information is available free of charge at https://pubs.acs.org/doi/10.1021/acscatal.5c01224.

Detailed chemical procedures; biotransformations; computational procedures; and spectral data as well as copies of NMR spectra (PNG) (PDF)

■ AUTHOR INFORMATION

Corresponding Author

Andreas Kirschning − *Institute of Organic Chemistry, Leibniz University Hannover, 30167 Hannover, Germany; Uppsala Biomedical Center (BMC), Uppsala University, 752 37 Uppsala, Sweden;* orcid.org/0000-0001-5431-6930; Email: andreas.kirschning@oci.uni-hannover.de

Authors

Jan Luca Budde − *Institute of Organic Chemistry, Leibniz University Hannover, 30167 Hannover, Germany*

Muhammed-Yasin Çay − *Institute of Organic Chemistry, Leibniz University Hannover, 30167 Hannover, Germany*

Gerald Dräger − *Institute of Organic Chemistry, Leibniz University Hannover, 30167 Hannover, Germany*

Jörn Droste − *Institute of Organic Chemistry, Leibniz University Hannover, 30167 Hannover, Germany*

Ahmed Hassanin − *Department of Bioorganic Chemistry, Leibniz Institute of Plant Biochemistry (IPB), 06120 Halle, Germany; Department of Pharmacognosy, Faculty of Pharmacy, Assiut University, 71526 Assiut, Egypt*

Mehdi D. Davari − *Department of Bioorganic Chemistry, Leibniz Institute of Plant Biochemistry (IPB), 06120 Halle, Germany;* orcid.org/0000-0003-0089-7156

Complete contact information is available at: https://pubs.acs.org/10.1021/acscatal.5c01224

Author Contributions

This manuscript was written through contributions of all authors. All authors have given approval to the final version of the manuscript.

Notes

The authors declare no competing financial interest.

■ ACKNOWLEDGMENTS

We thank Symrise AG (Mühlenfeldstraße 1, 37603 Holzminden, Germany) for financial support. A.H. is supported by a

Ph.D. scholarship from the Ministry of Higher Education of the Arab Republic of Egypt.

■ ABBREVIATIONS

PPTS=pyridinium *p*-toluenesulfonate; KHMDS=potassium hexamethyldisilazide; DIBAL-H=diisobutylaluminum hydride; LDA=lithium diisopropylamide; Ms=methylsulfonyl; DHP=dihydropyrane; THP=tetrahydropyranyl; *p*TsOH=*p*-tosylsulfonyl; DMS=dimethyl sulfide; NCS=*N*-chlorosuccinimide; DMSO=dimethyl sulfoxide

■ REFERENCES

(1) Ardkhean, R.; Caputo, D. F. J.; Morrow, S. M.; Shi, H.; Xiong, Y.; Anderson, E. A. Cascade polycyclizations in natural product synthesis. *Chem. Soc. Rev.* **2016**, *45*, 1557−1569.
(2) Yoder, R. A.; Johnston, J. N. A Case Study in Biomimetic Total Synthesis: Polyolefin Carbocyclizations to Terpenes and Steroids. *Chem. Rev.* **2005**, *105*, 4730−4756.
(3) The first coverage of the subject is found in Johnson, W. S. Biomimetic polyene cyclizations: A review. *Bioorg. Chem.* **1976**, *5*, 51−98.
(4) Johnson, W. S.; van der Gen, A.; Swoboda, J. J. New Structural and Stereochemical Aspects of the Cyclization of Olefinic Acetals. *J. Am. Chem. Soc.* **1967**, *89*, 170−172.
(5) Fish, P. V.; Johnson, W. S. The First Examples of Nonenzymic, Biomimetic Polyene Pentacyclizations. Total Synthesis of the Pentacyclic Triterpenoid Sophoradiol. *J. Org. Chem.* **1994**, *59*, 2324−2335.
(6) Corey, E. J.; Wess, G.; Xiang, Y. B.; Singh, A. K. Stereospecific total synthesis of (.+-.)-cafestol. *J. Am. Chem. Soc.* **1987**, *109*, 4717−4718.
(7) Corey, E. J.; Wood, H. B., Jr. A New Strategy for Stereocontrol of Cation-Olefin Cyclization. The First Chemical Emulation of the A/B-trans-9,10-syn-Folding Pathway of Steroid Biosynthesis from 2,3-Oxidosqualene. *J. Am. Chem. Soc.* **1996**, *118*, 11982−11983.
(8) Sakakura, A.; Ukai, A.; Ishihara, K. Enantioselective halocyclization of polyprenoids induced by nucleophilic phosphoramidites. *Nature* **2007**, *445*, 900−903.
(9) Zhang, Q.; Tiefenbacher, K. Terpene cyclization catalysed inside a self-assembled cavity. *Nat. Chem.* **2015**, *7*, 197−202.
(10) Zhang, Q.; Catti, L.; Pleiss, J.; Tiefenbacher, K. Terpene Cyclizations inside a Supramolecular Catalyst: Leaving-Group-Controlled Product Selectivity and Mechanistic Studies. *J. Am. Chem. Soc.* **2017**, *139*, 11482−11492.
(11) Némethová, I.; Schmid, D.; Tiefenbacher, K. Supramolecular Capsule Catalysis Enables the Exploration of Terpenoid Chemical Space Untapped by Nature. *Angew. Chem., Int. Ed.* **2023**, *62*, No. e202218625.
(12) Hart-Cooper, W. M.; Clary, K. N.; Toste, F. D.; Bergman, R. G.; Raymond, K. N. Selective monoterpene-like cyclization reactions achieved by water exclusion from reactive intermediates in a supramolecular catalyst. *J. Am. Chem. Soc.* **2012**, *134*, 17873−17876.
(13) Arnold, A. M.; Dullinger, P.; Biswas, A.; Jandl, C.; Horinek, D.; Gulder, T. Enzyme-like polyene cyclizations catalyzed by dynamic, self-assembled, supramolecular fluoro alcohol-amine clusters. *Nat. Commun.* **2023**, *14*, No. 813.
(14) Sokolova, D.; Piccini, G. M.; Tiefenbacher, K. Enantioselective Tail-to-Head Terpene Cyclizations by Optically Active Hexameric Resorcin[4]arene Capsule Derivatives. *Angew. Chem., Int. Ed.* **2022**, *61*, No. e202203384.
(15) Harms, V.; Kirschning, A.; Dickschat, J. Nature-Driven Approaches to Non-Natural Terpene Analogs. *Nat. Prod. Rep.* **2020**, *37*, 1080−1097.
(16) Yoshikuni, Y.; Ferrin, T. E.; Keasling, J. D. Designed divergent evolution of enzyme function. *Nature* **2006**, *440*, 1078−1082.
(17) Li, J.-X.; Fang, X.; Zhao, Q.; Ruan, J.-X.; Yang, C.-Q.; Wang, L.-J.; Miller, D. J.; Faraldos, J. A.; Allemann, R. K.; Chen, X.-Y.; Zhang, P. Rational engineering of plasticity residues of sesquiterpene synthases from *Artemisia annua*: product specificity and catalytic efficiency. *Biochem. J.* **2013**, *451*, 417−426.
(18) Christianson, D. W. Roots of biosynthetic diversity. *Science* **2007**, *316*, 60−61.
(19) Christianson, D. W. Structural and Chemical Biology of Terpenoid Cyclases. *Chem. Rev.* **2017**, *117*, 11570−11648.
(20) Wang, C.-M.; Hopson, R.; Lin, X.; Cane, D. E. Biosynthesis of the Sesquiterpene Botrydial in *Botrytis cinerea*. Mechanism and Stereochemistry of the Enzymatic Formation of Presilphiperfolan-8*β*-ol. *J. Am. Chem. Soc.* **2009**, *131*, 8360−8361.
(21) Oberhauser, C.; Harms, V.; Seidel, K.; Schröder, B.; Ekramzadeh, K.; Beutel, S.; Winkler, S.; Lauterbach, L.; Dickschat, J. S.; Kirschning, A. Exploiting the Synthetic Potential of Sesquiterpene Cyclases for Generating Unnatural Terpenoids. *Angew. Chem., Int. Ed.* **2018**, *57*, 11802−11806.
(22) Harms, V.; Ravkina, V.; Kirschning, A. Mechanistic similarities of sesquiterpene cyclases PenA, Omp6/7, and BcBOT2 are unraveled by an unnatural ″FPP-ether″ derivative. *Org. Lett.* **2021**, *23*, 3162−3166.
(23) Tran, C. D.; Dräger, G.; Struwe, H.; Siedenberg, L.; Vasisth, S.; Grunenberg, J.; Kirschning, A. Terpenoid cyclopropylmethyl diphosphates can serve as a substrates for the sesquiterpene synthase BcBOT2. *Org. Biomol. Chem.* **2022**, *20*, 7833−7839.
(24) Moeller, M.; Dhar, D.; Dräger, G.; Özbasi, M.; Struwe, H.; Wildhagen, M.; Davari, M. D.; Beutel, S.; Kirschning, A. The sesquiterpene cyclase BcBOT2 is able to promote Wagner-Meerwein-type migration of a methoxy group. *J. Am. Chem. Soc.* **2024**, *146*, 17838−17846.
(25) Struwe, H.; Li, H.; Schrödter, F.; Höft, L.; Fohrer, J.; Dickschat, J. S.; Kirschning, A. Telescoping a prenyltransferase and a diterpene synthase to transform unnatural FPP derivatives to new diterpenoids. *Org. Lett.* **2024**, *26*, 5888−5892.
(26) Struwe, H.; Droste, J.; Kirschning, A.; et al. Chemoenzymatic Synthesis of a New Germacrene Derivative named Germacrene F. *ChemBioChem* **2024**, *25*, No. e202300599.
(27) Struwe, H.; Grimm, C.; Beutel, S.; Kirschning, A.; Kara, S. Expanding the “terpenome”: Applications of unspecific peroxygenases (UPOs) in oxidations of unnatural terpenoids. *ChemCatChem* **2024**, No. e202401414.
(28) Struwe, H.; Nguyen, T.; Schwörer, S.; Droste, J.; Spinck, H.; Kirschning, A. Chemoenzymatic formation of oxa-terpenoids by sesqui- and diterpene synthase-mediated biotransformations with 9-oxy-FPP ether derivatives. *Biochemistry* **2025**, *64*, 498−508.
(29) Nikolaiczyk, V.; Irwan, J.; Nguyen, T.; Fohrer, J.; Elbers, P.; Schrank, P.; Davari, M. D.; Kirschning, A. Mutagenic reprogramming of the sesquiterpene synthase BcBOT2 provides new terpenes. *Cat. Sci. Technol.* **2023**, *13*, 233−244.
(30) Melching, S.; Bülow, N.; Wihstutz, K.; Jung, S.; König, W. A. Natural occurrence of both enantiomers of cadina-3,5-diene and *δ*-amorphene. *Phytochemistry* **1997**, *44*, 1291−1296.
(31) López-Gallego, F.; Wawrzyn, G. T.; Schmidt-Dannert, C.; et al. Sesquiterpene Synthases Cop4 and Cop6 from *Coprinus cinereus*: Catalytic Promiscuity and Cyclization of Farnesyl Pyrophosphate Geometric Isomers. *Appl. Environ. Microbiol.* **2010**, *11*, 7723−7733.
(32) Lopez-Gallego, F.; Agger, S. A.; Abate-Pella, D.; Distefano, M. D.; Schmidt-Dannert, C. Sesquiterpene Synthases Cop4 and Cop6 from *Coprinus cinereus*: Catalytic Promiscuity and Cyclization of Farnesyl Pyrophosphate Geometric Isomers. *ChemBioChem* **2010**, *11*, 1093−1106.
(33) Agger, S. A.; Lopez-Gallego, F.; Schmidt-Dannert, C. Diversity of sesquiterpene synthases in the basidiomycete *Coprinus cinereus*. *Mol. Microbiol.* **2009**, *72*, 1181−1195.
(34) Köllner, T. G.; Gershenzon, J.; Degenhardt, J. Molecular and biochemical evolution of maize terpene synthase 10, an enzyme of indirect defense. *Phytochemistry* **2009**, *70*, 1139−1145.
(35) Köllner, T. G.; Schnee, C.; Li, S.; Svatos, A.; Schneider, B.; Gershenzon, J.; Degenhardt, J. Protonation of a neutral (S)-*β*-bisabolene intermediate is involved in (S)-*β*-macrocarpene formation

https://doi.org/10.1021/acscatal.5c01224
ACS Catal. 2025, 15, 8125−8139

by the maize sesquiterpene synthases TPS6 and TPS11. *J. Biol. Chem.* **2008**, *283*, 20779−20788.
(36) Köllner, T. G.; O'Maille, P. E.; Gatto, N.; Boland, W.; Gershenzon, J.; Degenhardt, J. Two pockets in the active site of maize sesquiterpene synthase TPS4 carry out sequential parts of the reaction scheme resulting in multiple products. *Arch. Biochem. Biophys.* **2006**, *448*, 83−92.
(37) Harms, V.; Schröder, B.; Oberhauser, C.; Tran, C. D.; Winkler, S.; Dräger, G.; Kirschning, A. Methyl-shifted farnesyldiphosphate derivatives are substrates for sesquiterpene cyclases. *Org. Lett.* **2020**, *22*, 4360−4365.
(38) Davisson, V. J.; Neal, T. R.; Poulter, C. D. Farnesyl-Diphosphate Synthase. Catalysis of an Intramolecular Prenyl Transfer with Bisubstrate Analogs. *J. Am. Chem. Soc.* **1993**, *115*, 1235−1245.
(39) Imamura, Y.; Takikawa, H.; Sasaki, M.; Mori, K. Triterpenoid total synthesis. Synthesis and absolute configuration of mispyric acid. *Org. Biomol. Chem.* **2004**, *2*, 2236−2244.
(40) Orita, A.; Watanabe, A.; Tsuchiya, H.; Otera, J. Integrated chemical process. Construction of highly substituted allylic moieties from allylic sulfones in one-pot. *Tetrahedron* **1999**, *55*, 2889−2898.
(41) Xie, J.; Zheng, Z.; Liu, X.; Zhang, N.; Choi, S.; He, C.; Dong, G. Asymmetric total synthesis of (+)-phainanoid A and biological evaluation of the natural product and its synthetic analogues. *J. Am. Chem. Soc.* **2023**, *145*, 4828−4852.
(42) Johnson, W. S.; Werthemann, L.; Bartlett, W. R.; Brocksom, T. J.; Li, T.-T.; Faulkner, D. J.; Petersen, M. R. Simple stereoselective version of the Claisen rearrangement leading to trans-trisubstituted olefinic bonds. Synthesis of squalene. *J. Am. Chem. Soc.* **1970**, *92*, 741−743.
(43) Khalilov, L. M.; Khalilova, A. Z.; Odinokov, V. N.; Baltaev, U. A.; Paramonov, E. A.; Dzhemilev, U. M. Identification and biological activity of the volatile organic substances emitted by plants and insects II. Sesquiterpene composition of the native scent of leaves of the potato *Solanum tuberosum*. *Chem. Nat. Compd.* **1999**, *35*, 422−426.
(44) Karplus, M. Vicinal Proton Coupling in Nuclear Magnetic Resonance. *J. Am. Chem. Soc.* **1963**, *85*, 2870−2871.
(45) Tomita, T.; Kim, S.-Y.; Teramoto, K.; Meguro, A.; Ozaki, T.; Yoshida, A.; Motoyoshi, Y.; Mori, N.; Ishigami, K.; Watanabe, H.; Nishiyama, M.; Kuzuyama, T. Structural Insights into the CotB2-Catalyzed Cyclization of Geranylgeranyl Diphosphate to the Diterpene Cyclooctat-9-en-7-ol. *ACS Chem. Biol.* **2017**, *12*, 1621−1628.
(46) Ma, G.-H.; Chen, K.-X.; Zhang, J.-Q.; Li, Y.-M. Advance in biological activities of natural guaiane-type sesquiterpenes. *Med. Chem. Res.* **2019**, *28*, 1339−1358.
(47) Barra, L.; Schulz, B.; Dickschat, J. S. Pogostol biosynthesis by the endophytic fungus *Geniculosporium*. *ChemBioChem* **2014**, *15*, 2379−2383.
(48) Brody, E. P.; Gutsche, C. D. The mechanism of the acid-catalyzed decomposition of the farnesyl phosphates. *Tetrahedron* **1977**, *33*, 723−729.
(49) Tantillo, D. J. Biosynthesis via carbocations: theoretical studies on terpene formation. *Nat. Prod. Rep.* **2011**, *28*, 1035−1053.
(50) Hare, S. R.; Tantillo, D. J. Dynamic behavior of rearranging carbocations - implications for terpene biosynthesis. *Beilstein J. Org. Chem.* **2016**, *12*, 377−390.
(51) Major, D. T.; Weitman, M. Electrostatically guided dynamics-the root of fidelity in a promiscuous terpene synthase? *J. Am. Chem. Soc.* **2012**, *134*, 19454−19462.
(52) Siebert, M. R.; Zhang, J.; Addepalli, S. V.; Tantillo, D. J.; Hase, W. L. The need for enzymatic steering in abietic acid biosynthesis: gas-phase chemical dynamics simulations of carbocation rearrangements on a bifurcating potential energy surface. *J. Am. Chem. Soc.* **2011**, *133*, 8335−8343.
(53) Siebert, M. R.; Manikandan, P.; Sun, R.; Tantillo, D. J.; Hase, W. L. Gas-Phase Chemical Dynamics Simulations on the Bifurcating Pathway of the Pimaradienyl Cation Rearrangement: Role of Enzymatic Steering in Abietic Acid Biosynthesis. *J. Chem. Theory Comput.* **2012**, *8*, 1212−1222.
(54) Hong, Y. J.; Tantillo, D. J. Biosynthetic consequences of multiple sequential post-transition-state bifurcations. *Nat. Chem.* **2014**, *6*, 104−111.
(55) Raz, K.; Levi, S.; Gupta, P. K.; Major, D. T. Enzymatic control of product distribution in terpene synthases: insights from multiscale simulations. *Curr. Opin. Biotechnol.* **2020**, *65*, 248−258.
(56) Major, D. T.; Freud, Y.; Weitman, M. Catalytic control in terpenoid cyclases: multiscale modeling of thermodynamic, kinetic, and dynamic effects. *Curr. Opin. Chem. Biol.* **2014**, *21*, 25−33.
(57) Tantillo, D. J. Interrogating chemical mechanisms in natural products biosynthesis using quantum chemical calculations. *WIREs Comput. Mol. Sci.* **2020**, *10*, No. e1453.
(58) Vögeli, B.; Erb, T. J. "Negative" and "positive catalysis": complementary principles that shape the catalytic landscape of enzymes. *Curr. Opin. Chem. Biol.* **2018**, *47*, 94−100.
(59) Klucznik, T.; Syntrivanis, L.-D.; Baś, S.; Mikulak-Klucznik, B.; Moskal, M.; Szymkuć, S.; Mlynarski, J.; Gadina, L.; Beker, W.; Burke, M. D.; Tiefenbacher, K.; Grzybowski, B. A. Computational prediction of complex cationic rearrangement outcomes. *Nature* **2024**, *625*, 508−515.
(60) Chemical Computing Group ULC. *Molecular Operating Environment (MOE)*; Chemical Computing Group ULC: Montreal, QC, 2024.
(61) Lou, T.; Li, A.; Xu, H.; Pan, J.; Xing, B.; Wu, R.; Dickschat, J. S.; Yang, D.; Ma, M. Structural insights into three sesquiterpene synthases for the biosynthesis of tricyclic sesquiterpenes and chemical space expansion by structure-based mutagenesis. *J. Am. Chem. Soc.* **2023**, *145*, 8474−8485.

https://doi.org/10.1021/acscatal.5c01224
ACS Catal. 2025, 15, 8125−8139